remote sensing

MDPI

Article

Automatic Flood Duration Estimation Based on Multi-Sensor Satellite Data

Michaela Rättich, Sandro Martinis * and Marc Wieland

German Aerospace Center (DLR), German Remote Sensing Data Center (DFD),
82234 Oberpfaffenhofen, Germany; michaela.raettich@dlr.de (M.R.), marc.wieland@dlr.de (M.W.)
* Correspondence: sandro.martinis@dlr.de (S.M.)

Received: 02 January 2020; Accepted: 12 February 2020; Published: 14 February 2020

Abstract: Flood duration is a crucial parameter for disaster impact assessment as it can directly influence the degree of economic losses and damage to structures. It also provides an indication of the spatio-temporal persistence and the evolution of inundation events. Thus, it helps gain a better understanding of hydrological conditions and surface water availability and provides valuable insights for land-use planning. The objective of this work is to develop an automatic procedure to estimate flood duration and the uncertainty associated with the use of multi-temporal flood extent masks upon which the procedure is based. To ensure sufficiently high observation frequencies, data from multiple satellites, namely Sentinel-1, Sentinel-2, Landsat-8 and TerraSAR-X, are analyzed. Satellite image processing and analysis is carried out in near real-time with an integrated system of dedicated processing chains for the delineation of flood extents from the range of aforementioned sensors. The skill of the proposed method to support satellite-based emergency mapping activities is demonstrated on two cases, namely the 2019 flood in Sofala, Mozambique and the 2017 flood in Bihar, India.

Keywords: flood monitoring; flood duration; Sentinel-1; Sentinel-2; Landsat-8; TerraSAR-X

1. Introduction

Floods can be considered the most frequent, disastrous and widespread natural hazard [1–5], accounting for more than 43% of all disaster events recorded globally between 1998 and 2017. Consequently, floods have adversely affected an estimated two billion people, causing notable structural damages and resulting in significant economic losses [6]. Flood monitoring is important for effective disaster risk management, in particular, for emergency response, recovery and preparedness actions [2,7]. During the emergency response phase, near real-time information about the flood water extent and the flood duration are among the most instrumental to help effectively mobilize and distribute often finite resources to priority areas. Similarly, in the recovery and preparedness phases, water extent and duration information provide valuable inputs for insurance claims management, land-use planning and an improved understanding of hydrological conditions. Remote sensing is increasingly being used for flood monitoring as it provides a cost effective form of surveillance over large areas with potentially high temporal revisit periods [8]. In particular, the recently launched Copernicus Sentinel satellites of the European Commission show great potential for flood monitoring. This is attributed to the high temporal and spatial resolutions of cost-free Sentinel data and the systematic acquisition capabilities of the sensors. Flood duration estimation generally refers to time-series analysis of binary flood extent masks to derive a spatially explicit map that illustrates the length of time for which each pixel has been flooded during a pre-defined time range. Its accuracy is, therefore, directly correlated with the quality of the flood extent maps that are used as inputs for the computation. The time between successive valid observations (pixels that are not covered by clouds, cloud shadows or otherwise marked as no-data) in the time-series is a

function of the satellite acquisition plan and the presence of clouds in optical data. These two sources introduce further uncertainties to any resultant flood duration product.

Numerous methods have been developed to derive flood extents from satellite data. Existing methods can be classified as rule-based and machine learning methods. While rule-based methods have returned viable results with acceptable levels of accuracy for specific sensors, the lack of methodological transferability between sensors [9,10] has been highlighted. Furthermore, few studies have presented robust solutions that have been demonstrated across different geographic and scene properties [11–13]. Recently, convolutional neural networks have been applied to flood monitoring; features are learned directly from raw images by combining convolutional and pooling layers. First results reported notably higher accuracies and generalizability compared to rule-based and classical machine learning approaches with hand-crafted features [14–16]. While a more detailed review of flood extent mapping methods is beyond the scope of this study, the most commonly used methods can be found in Klemas [17] and Lin et al. [18].

Compared to the extensive quantity of literature on flood extent mapping, only a few studies focus on the estimation of flood duration. Most of the studies obtain flood extent masks from Synthetic Aperture Radar (SAR) data as those observations are independent of prevailing weather conditions and can be acquired during both day and night [19]. For instance, Bhatt et al. [20] used a manual GIS-based raster analysis to derive flood duration from a time-series of Radar Imaging Satellite 1 (RISAT-1) and Radarsat-2 images. Rahman et al. [21] determined flood duration as a factor for a flood susceptibility study in Bangladesh in 2017 using four satellite images from the Advanced Land Observing Satellite-2 (ALOS-2), Phased Array L-band Synthetic Aperture Radar (PALSAR) and Sentinel-1. The resultant flood duration layer is highly aggregated and abstracted into categorical classes. Ramsey et al. [22] used eight Environmental Satellite Advanced Synthetic Aperture Radar (Envisat ASAR) images to derive flood masks to monitor wetlands at 20 day intervals. O'Hara et al. [23] examined 33 Sentinel-1 images to map flood duration in Ireland, expressed in terms of flood frequency (i.e., the number of times a pixel is classified as flooded over a six-month period). Kundu et al. [24] compared two flood disasters in Odisha (India) with eight Radarsat-1 observations, categorizing the areas by duration based on the length of time successive flood extent masks could be empirically extracted. Rahman and Thakur [25] used four Radasat-1 scenes to derive flood masks with a threshold-based method and superimposed them to analyze the duration of the 2008 flood event in Kendrapara District (Orissa State, India). Few methods use optical satellite data for flood duration estimation. Zhang et al. [26] used a shape metamorphosis method to obtain the flood duration from flood masks generated with a threshold-based technique from three Gaofen-1 (GF-1) satellite images. Kumar [27] used a locational probability model [28] to analyze the flood duration of the 2014 floods in Jammu and Kashmir from Landsat-7 and Landsat-8 data. Kurte [29] used five Worldview-2 images to map the flood duration in Srinagar City (Kashmir, India) in 2014. To overcome the limitation of optical data due to potential cloud coverage in individual images, Islam et al. [30] estimated the duration of two major floods in 2004 and 2007 in Bangladesh based on MODIS eight-day composite products. While this approach effectively reduces the influence of clouds on the interpretability of available images, it requires working with temporally aggregated weekly products, rather than at a finer temporal resolution or with daily data.

Based on a recent literature review, we observed a general lack of description of flood duration estimation methods. The majority of post studies focus on single sensors or sensor groups (SAR or optical) to derive flood extent masks, which result in lengthy time gaps between sequential observations. Consequently, higher uncertainties are introduced into these flood duration estimates. Temporal aggregation at the dataset level to overcome partial visibility due to cloud coverage further increases this limitation. Despite the importance of temporal resolution on time-series analysis, particularly in highly dynamic surface water environments, flood duration uncertainty has not been previously considered in the literature to the best of the authors' knowledge. Further research is needed to better understand and to quantify uncertainties related to the temporal revisit periods of satellites and with respect to the partial visibility in optical data due to atmospheric

effects. Furthermore, almost all of the aforementioned studies estimate flood durations with manual GIS-based operations over a limited number of scenes. These methods would not be optimal for the analyses of longer time-series characterized by a larger number of scenes.

The objective of this study is, therefore, to develop, formalize and describe a method to automatically estimate flood duration from multiple sources of satellite images. The flood duration estimation method is built on existing processing chains that extract near real-time flood masks from Sentinel-1, Sentinel-2, Landsat-8 and TerraSAR-X. Thus, it is designed to provide the highest possible temporal resolution by combining systematically acquired SAR and optical imagery with on-demand data from the tasked TerraSAR-X satellite. To quantify the effects of applying the proposed multi-source approach, we explicitly treat duration uncertainty by considering the influence of the temporal revisit period of the satellites, the distribution of observations and the presence of invalid pixels (e.g., pixels temporary covered by clouds). The study is structured as follows: In the next section, we describe the study areas and data. In the subsequent sections, we provide a brief summary of the processing chains for flood extent mapping. The flood duration estimation method is described, and the results of the method demonstrated over the two study areas are presented. Finally, the discussion highlights both the advantages and challenges of the proposed method, and conclusions are drawn accordingly.

2. Study Areas and Data

The developed methodology was tested in two study areas. The first one is located in Sofala province, Mozambique (coordinates: UL: 33.973°, –19.105°; LR: 34.993°, –20.342°) and covers an area of 100 x 140 km² (Figure 1). The region was severely affected by tropical cyclone Idai in March 2019. Cyclone Idai made landfall near Beira City on 15/03/2019, causing devastating storm damages and severe flooding. It is considered to be one of the worst tropical cyclones that has hit Africa and the whole Southern Hemisphere, and caused more than 600 fatalities and left around 1.85 million people in need in Mozambique alone [31].

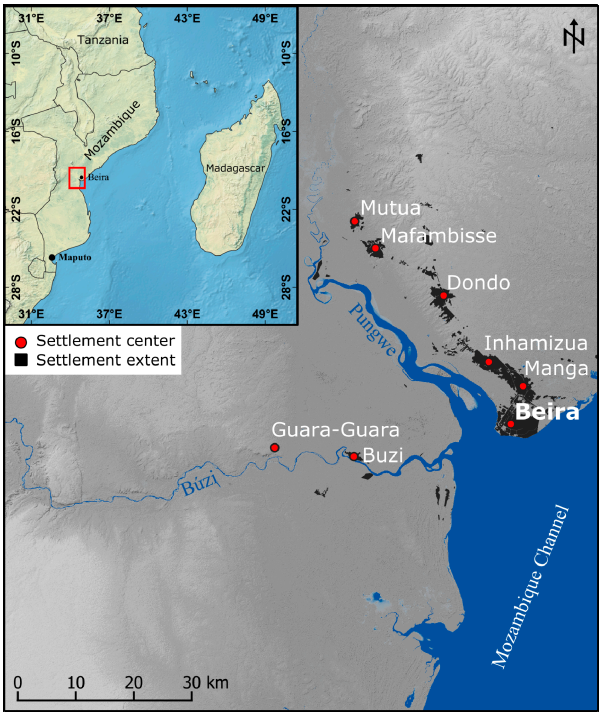

Figure 1. Overview of the study area in Mozambique. The map layers include the hillshade in the background, which was generated from the Shuttle Radar Topography Mission (SRTM) [32], open water bodies data [13] and map data © OpenStreetMap contributors.

Seventy-six satellite images were acquired from different sensors over the study area between 02/03/2019 and 07/04/2019. In particular, the acquisitions include the following: 33 Sentinel-1 Ground Range Detected (GRD) Interferometric Wide Swath (IW) scenes acquired over 11 days with spatial resolutions of ~20 m, 36 Sentinel-2 L1C image tiles from the Multispectral Instrument (MSI) with a spatial resolution of 10–20 m, 5 TerraSAR-X scenes in ScanSAR mode acquired over 4 days with a spatial resolution of 18.5 m and 2 Landsat-8 scenes acquired with the Operational Land Imager (OLI) over 1 day with a spatial resolution of 30 m. Figure 2 provides an overview of the observation dates of all of the aforementioned acquisitions used for the flood duration estimation in Mozambique.

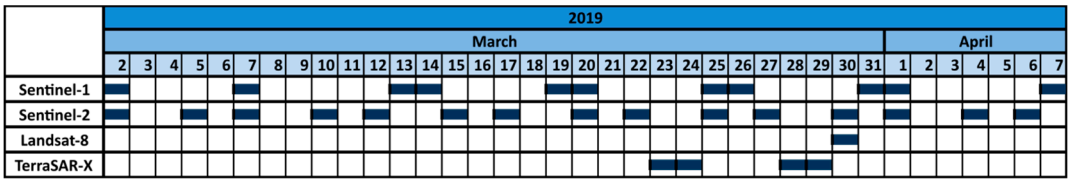

Figure 2. Temporal coverage of Sentinel-1, Sentinel-2, TerraSAR-X and Landsat-8 data acquired over the study area of Mozambique during the period of interest.

The second study area is located in the state of Bihar in northeastern India (coordinates: UL: 85.522°, 26.084°; LR: 87.043°, 25.244°) and covers an area of 150 x 90 km² (Figure 3). Bihar is seasonally affected by tropical monsoon rains and is considered to be one of the most flood prone regions in the country. The highest water levels are usually recorded between June and October. This study covers a time period when torrential rainfall in the foothills of the Himalayas in Nepal led to damaging floods in several rivers located within the study area.

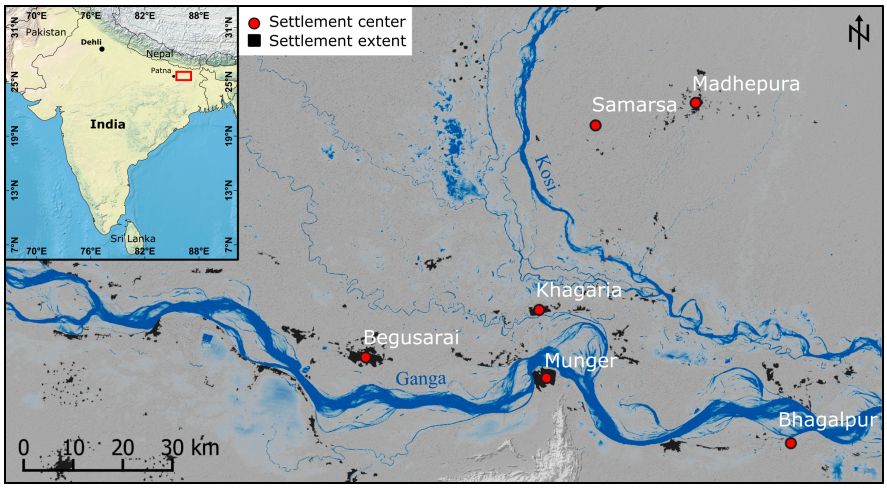

Figure 3. Overview of the study area in Bihar, India. The map layers include the hillshade in the background, which was generated from SRTM [32], open water bodies data [13] and map data © OpenStreetMap contributors.

Thirty-nine satellite images were acquired from Sentinel-1, Sentinel-2 and Landsat-8 between 03/07/2017 and 28/09/2017.This includes 15 Sentinel-1 GRD IW scenes acquired with a spatial resolution of ~20 m over 15 days, 14 Sentinel-2 MSI scenes with a spatial resolution of 10–20 m and 10 Landsat-8 OLI scenes acquired with a spatial resolution of 30 m over 5 days. Only Sentinel-2 tiles with cloud coverage of less than 70% were considered. TerraSAR-X acquisitions were not available during this observation period of interest (Figure 4).

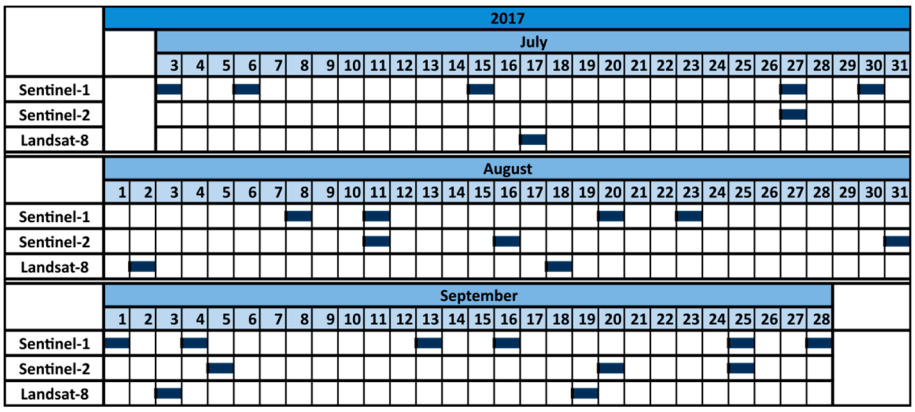

Figure 4. Temporal coverage of Sentinel-1, Sentinel-2 and Landsat-8 data acquired over the study area of Bihar during the period of interest.

3. Method

3.1. Flood Extent

Inputs for the flood duration estimation were derived with the automatic and operational system of the German Aerospace Center (DLR), which is designed for near real-time flood extent mapping with multi-sensor satellite data. The system is based on four processing chains for the derivation of flood extents from Sentinel-1 and TerraSAR-X radar data, as well as from optical Sentinel-2 and Landsat data. The collection of the Sentinel-1, Sentinel-2 and Landsat-8 data is systematically acquired and enables continuous monitoring of floodplains at intervals of a few days. In contrast, the TerraSAR-X flood service must be activated on demand in the case of a flood situation but can acquire images at higher spatial and temporal resolutions. All processing chains include the following generic steps: data acquisition and ingestion, pre-processing, adaptation of global auxiliary data (e.g., digital elevation models, topographic slope information and topographic indices, as well as reference water masks), image classification and the dissemination of flood extent products via web services. An overview of the system is illustrated in Figure 5.

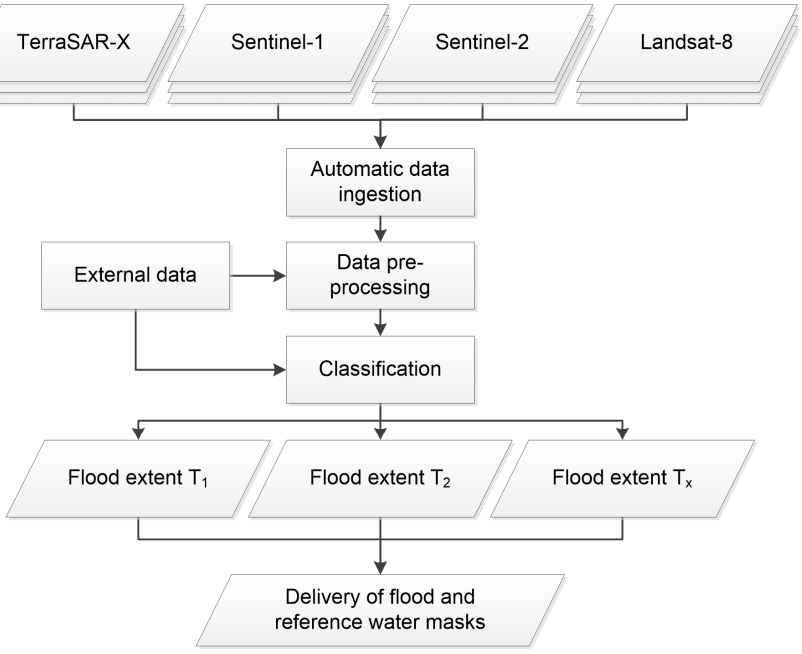

Figure 5. Overview of German Aerospace Center's (DLR) satellite-based flood monitoring system used to extract flood extent information products in near real-time from multiple satellite image sources.

Water extraction with TerraSAR-X and Sentinel-1 data is based on a hierarchical tile-based thresholding method that is coupled with a fuzzy-logic post-classification refinement step [11,12,33]. Additionally, Sentinel-1 pre-event time-series data are used to compute a sand exclusion layer, which reduces overestimations of the water extent due to permanent sand surfaces with similar low backscatter values [34]. The exclusion layer is subtracted from the computed water mask to eliminate areas that exhibit low backscatter over longer periods of time. A globally trained convolutional neural network is used to extract water extents with Sentinel-2 and Landsat imagery [16]. The network specifically handles clouds and cloud shadows to generate a mask without the consideration of these artefacts and thereby remove potential bias from any downstream analysis. Independent of the applied method and data sources for water extraction, it is essential to distinguish between temporary and permanently flooded areas. For this purpose, a reference water mask was used to approximate the typical water extent for a given time-period. Consequently, the set difference between the water and reference water masks represents temporarily flooded areas. In order to achieve global coverage, the reference water mask is generated from a combination of different data sources, namely the Shuttle Radar Topography Mission (SRTM) Water Body Data (SWBD) and the MODIS land–water mask (MOD44W), which is used for all northern and southern latitudes beyond the SWBD data coverage extent [35]. For some countries, seasonal reference water masks based on Sentinel-2 and Landsat time-series are also computed. These masks are used instead of the SWBD and MODIS reference water masks upon availability, since they are more up-to-date and consider seasonal effects. The processing chains are described in more detail in [11,12,16,33,34,36,37]. Figure 6 shows examples of input data and the resulting flood extent masks generated over the study area in Mozambique.

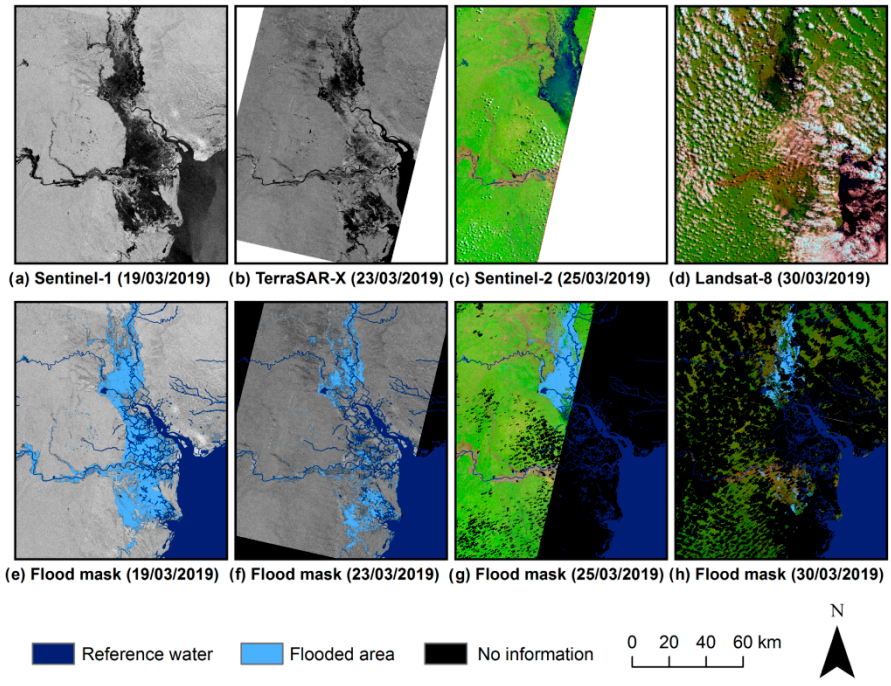

Figure 6. Sample results from the automatic multi-sensor flood mapping system over the study area in Mozambique. (**a**) Sentinel-1 data from 19/03/2019 (© COPERNICUS by the European Union and European Space Agency); (**b**) TerraSAR-X from 23/03/2019 (© DLR); (**c**) Sentinel-2 (RGB: SWIR–NIR-Blue) from 25/03/2019 (© COPERNICUS by the European Union and European Space Agency); (**d**) Landsat-8 data (RBG: SWIR–NIR–Blue) from 30/03/2019 (© USGS); (**e–h**) single-temporal flood masks, valid pixel masks and reference water masks.

The quality of any flood duration product depends directly on the accuracy of the flood extent masks used as inputs. The respective performances of the processing chains for flood extent mapping have been evaluated against globally distributed reference datasets in previous studies. For Sentinel-1, values between 0.88 and 0.91 were reported for Cohen's Kappa coefficient (κ) [11]; tests for TerraSAR-X resulted in producer accuracies between 0.83 and 0.98 and user accuracies between 0.95 and 0.98 [12]; the flood extent masks derived by the Sentinel-2/Landsat flood processor achieved κ values between 0.86 and 0.97 [16].

3.2. Flood Duration

Flood duration estimation was carried out by time-series analysis of binary flood extent masks to derive a spatially explicit map that describes for how long each pixel has been flooded during a pre-defined time range. In principal, flood extent masks from any source can be used as input. To facilitate the automation of the procedure to transform raw data into final products, we built on the aforementioned flood monitoring system to extract flood extents from Sentinel-1, Sentinel-2, Landsat-8 and TerraSAR-X data. Independent of the source and the method, all input masks needed to be binary coded (0 = no flood, 1 = flood). If the images contained invalid pixels attributed to cloud coverage and cloud-shadows in optical data or due to no data values at image boundaries, a corresponding valid mask (0 = invalid, 1 = valid) needed to be computed, where these pixels were identified. Figure 7 shows the workflow applied to estimate flood duration. Flood extent masks are requisite inputs, along with a pre-defined area of interest and additional processing parameters (i.e., spatial resolution, coordinate reference system and time period). During pre-processing, all input datasets were aligned with the same coordinate reference system, spatial extent and resolution; this was achieved with reprojection, resampling, clipping and mosaicking (merging) operations. At this stage, valid masks were generated from satellite image footprints, in the case that they were unavailable prior to the analysis. The preprocessed flood and valid masks were stacked along the time axis with the most recent acquisition date to the right. This temporal stack served as input to a time-series analysis, where start and end dates of all flood periods and observation gaps were identified for each pixel. This information was used to derive two different types of flood duration products, namely the Total Flood Duration (TFD) and the Backward Flood Duration (BFD). Furthermore, a quality layer was produced to quantify the uncertainty related to the duration products based on observation density and distribution.

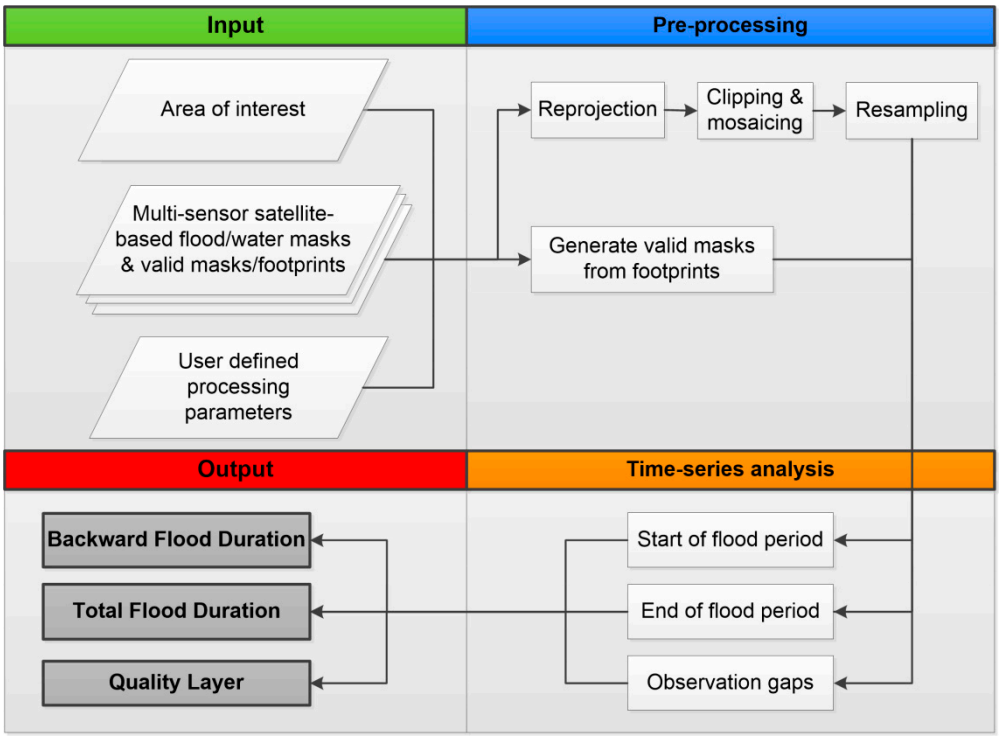

Figure 7. Workflow of the flood duration estimation processor.

Total Flood Duration is computed for each pixel within a defined time period, which may cover more than a single flood event. Figure 8 shows a schematic illustration of the approach that was applied to compute the Total Flood Duration of a single pixel over a period of 20 days (D1–D20). The blue boxes mark dates when the pixel was identified as being flooded, whereas the grey boxes indicate dates when floods were undetected. The white boxes represent days without an observation at a particular pixel location; this may be due to either the pixel being marked as invalid or because there was a lack of available satellite imagery on the given day. In this study, we defined a "flood period" as a length of time characterized by successive and uninterrupted flood detection. Changes from "no flood" to "flood" mark the start of a flood period and changes from "flood" to "no flood" identify its end. We assumed that a pixel remained flooded on days without satellite observations when these days fell between two days with flood detections.

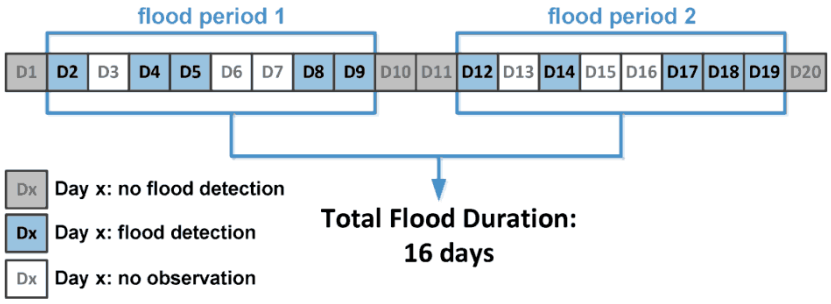

Figure 8. Example of Total Flood Duration computation for a single pixel across a period of 20 days.

The duration of each flood period can be computed, in days, between its start and end date. Hence, Total Flood Duration (TFD) is defined as the sum of the durations of all flood periods within a given time period and can be calculated for a single pixel i as follows:

$$TFD_i = \sum_{f=1,n} D_{f,end} - D_{f,start} \quad (1)$$

where f is the index accounting for n flood periods, and $D_{f,start/end}$ is either the start or the end date of the respective flood period.

Backward Flood Duration (BFD) is a special case of the Total Flood Duration and only considers for how long a location has been flooded in the most recent (current) flood period. The BFD computation for a single pixel i is illustrated in Figure 9 and can be described with the following formula:

$$BFD_i = D_{current,end} - D_{current,start} \quad (2)$$

where $D_{current,start/end}$ denotes the start of the current flood period and its end, which coincides with the most recent acquisition date in this example.

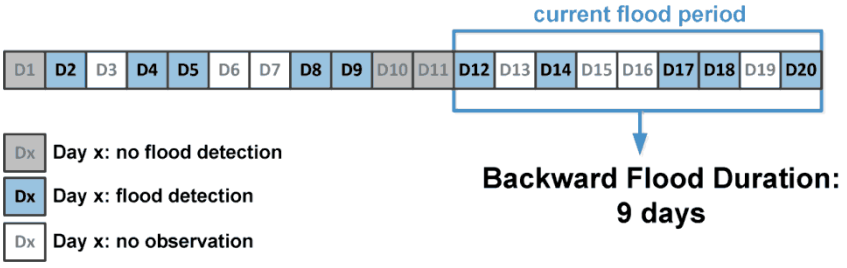

Figure 9. An example of a Backward Flood Duration computation for a single pixel across a time period of 20 days.

The quality of the flood duration products does not only depend on the accuracy of the flood extent masks used as inputs for the time-series but is also strongly influenced by the observation frequency and observation distribution. To quantify this sensitivity, we introduced a quality metric that accounts for the observation frequency and the distribution of valid observations before, during and after a flood period. Figure 10 and Equations (3)–(6) illustrate the computation of this quality metric.

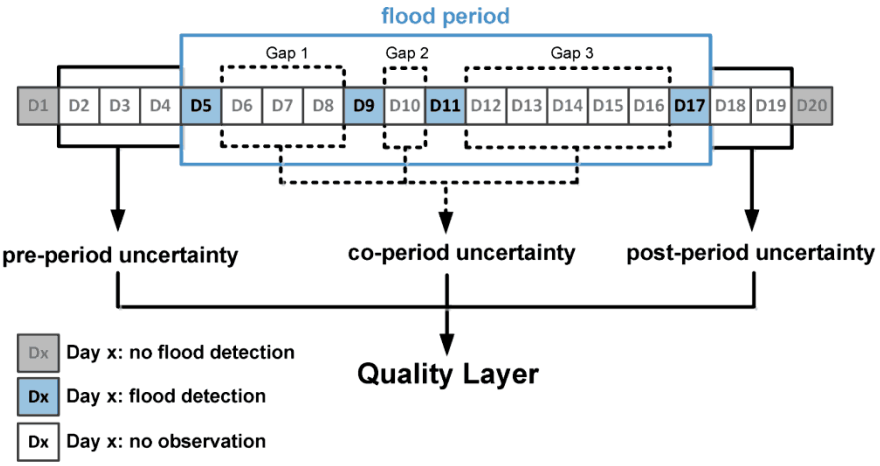

Figure 10. Example of a quality metric computation associated with the flood duration estimation of a single pixel across a time period of 20 days.

The pre-period and post-period uncertainties reflect the quality of the estimates at the start and the end of the flood periods, whereas the co-period uncertainty is associated with the uncertainty during or within the flood period. The quality layer QL_i can be calculated for each pixel i as a sum of all of the pre-, co- and post-period uncertainties as follows:

$$QL_i = \sum_{f=1,n} PreU_i + CoU_i + PostU_i \quad (3)$$

where $PreU_i$, CoU_i *and* $PostU_i$ are the respective pre-, co- and post-period uncertainties of the observed period, where:

$$PreU_i = D_{i,start} - D_{i,before} \quad (4)$$

$$CoU_i = \sum_{g=1,m} ((D_{g,end} - D_{g,start})^2 + (D_{g,end} - D_{g,start})) * 0.5)/m \quad (5)$$

$$PostU_i = D_{i,after} - D_{i,end} \quad (6)$$

The pre-period uncertainty is calculated by subtracting the date of the first no flood detection before the flood period, $D_{i,before,}$ from the date, indicating the start of the flood period, $D_{i,start}$. The calculation of the post-period uncertainty, $PostU_i$, is the difference between the date of the first no flood detection after the flood period and the date of the end of the flood period. The CoU_i is a weighted average of a number of m observation gaps g. $D_{g,start}$ is the first day without information after a day with flooding in gap g and $D_{g,end}$ is the first day with flooding after this gap. As a result, longer observation gaps are penalized with higher uncertainties.

The unitless quality layer can be used as an indicator of the relative quality of a flood duration product for each pixel. Furthermore, the averaging of CoU_i by m enables the unitless values of QL_i of different flood events with variable flood durations and within different study sites to be easily compared. Otherwise, longer flood events would be assigned lower performing quality values than shorter ones, which would reduce the interpretability of this product.

4. Results

4.1. Mozambique

Figure 11 depicts the Total Flood Duration computed for the study area in Mozambique during the 02/03/2019–07/04/2019 observation period. The TFD product was derived from Sentinel-1/2, TerraSAR-X and Landsat-8 data and computed with a pixel spacing of 10 m. The product showed extensive areas with flood durations of 14–20 days in the southern and northern parts along the Pungwe River. The area along the Búzi River showed flood durations of 1–10 days, with parts that remained flooded for as long as 25 days. In addition, some smaller areas appeared to be flooded for the entire period (37 days), which may be attributed to the quality of the reference water mask used. In particular, the reference water extent was based on a combination of SWBD and data from the Humanitarian OpenStreetMap Team (HOT).

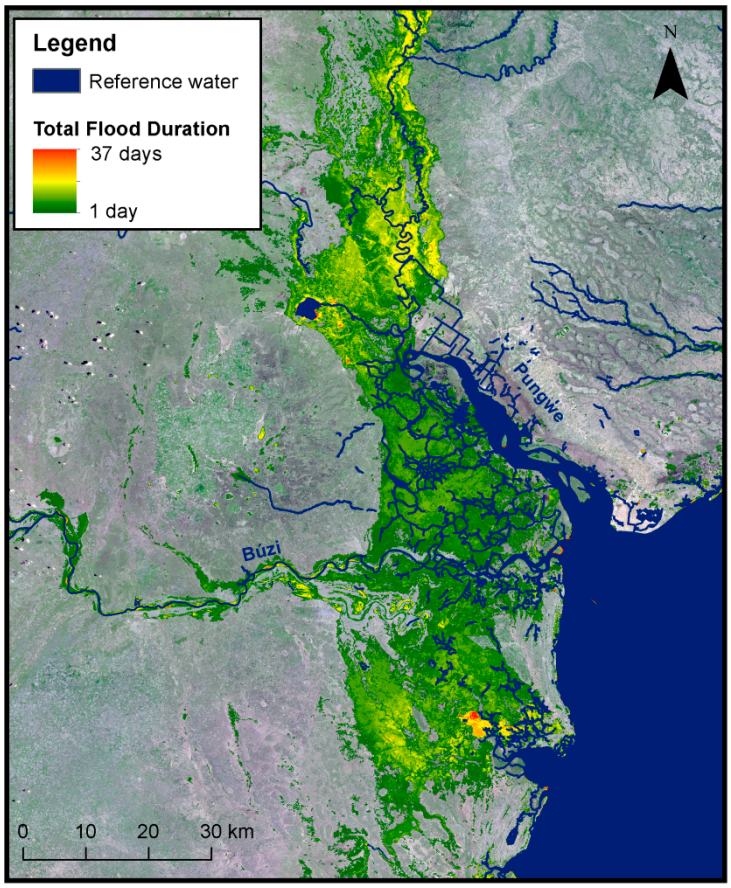

Figure 11. The map illustrates the Total Flood Duration calculated over the study area in Mozambique for the 02/03/2019–07/04/2019 observation period. The reference water extent is based on SRTM Water Body Data SWBD and data from the Humanitarian OpenStreetMap Team HOT. A mosaic of four Sentinel-2 tiles (RGB) acquired on 02/12/2018 and 02/12/2018 is used as a background.

The corresponding quality layer is presented in Figure 12a. It supports the performance of a relative quality comparison associated with pixels within the corresponding flood duration product. In most areas, relatively low uncertainty values of <10 could be achieved. Figure 13 shows the histogram of the Total Flood Duration quality based on flood coverage. The median value of the quality layer related to the flood duration product was 6, which was assigned to the majority of the pixels, comprising of an area of ~570 km². In order to demonstrate the influence of the observation frequency on the quality of the resultant TFD, the respective quality layer was calculated for the same observation period, based on flood masks derived from radar observations alone (Sentinel-1 and TerraSAR-X). The resulting uncertainty values are visualized in Figure 12b and 13 and show an increased uncertainty associated with the flood duration product. A general shift of the pixels to higher uncertainty values can be observed in Figure 13. Areas with an increase to values between 13 and 25 could be observed, and the median value of the quality layer increased from 6 to 8. This

demonstrated that the quality of flood duration estimation could be improved with an increased observation rate, which is possible with the use of hybrid information from different data sets.

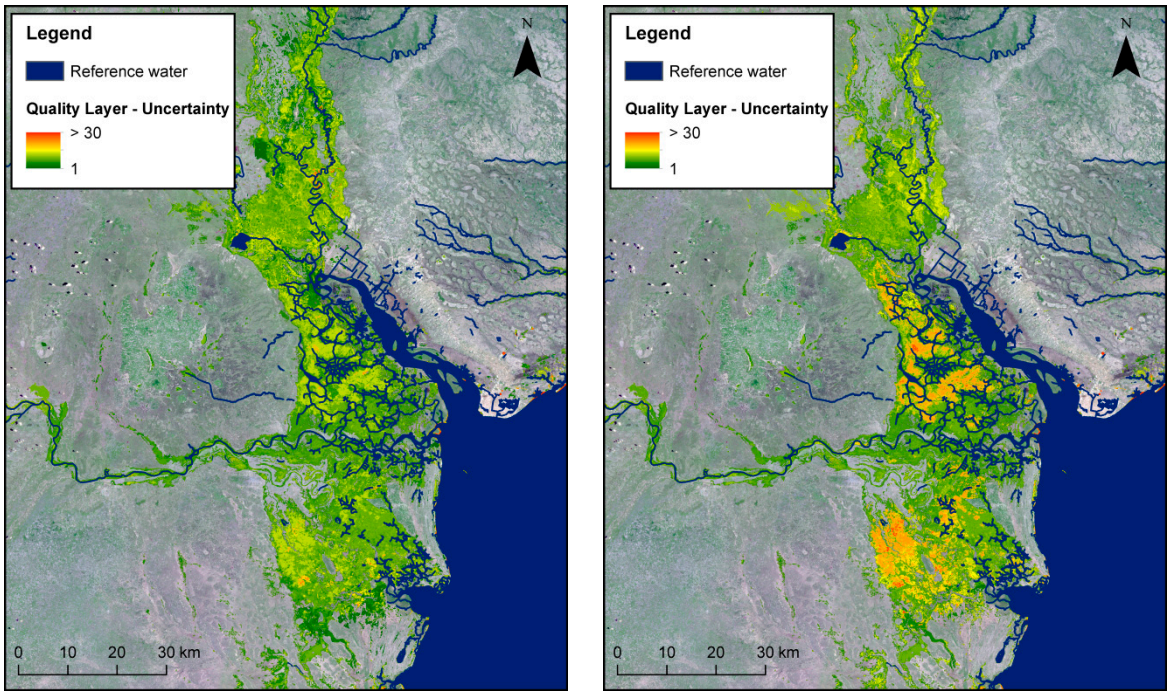

Figure 12. Flood duration quality layers computed for different data availability scenarios. (**a**) Flood duration quality layer using all available data (Sentinel-1, TerraSAR-X, Sentinel-2 and Landsat-8); (**b**) Flood duration quality layer using only radar data (Sentinel-1 and TerraSAR-X) for the 02/03/2019–07/04/2019 observation period. The reference water extent is based on SWBD and data from HOT. A mosaic of four Sentinel-2 tiles (RGB) acquired on 02/12/2018 and 02/12/2018 is used as a background.

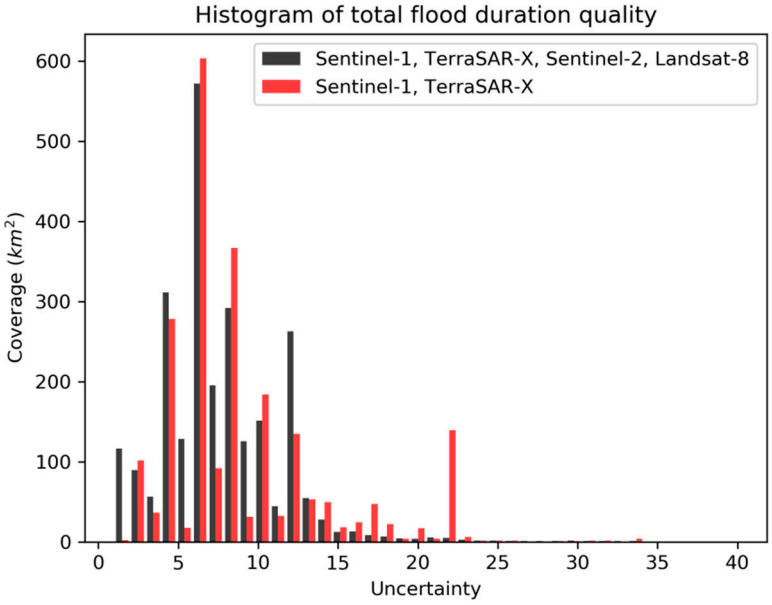

Figure 13. Histogram of the Total Flood Duration quality layer demonstrated on the case in Mozambique and based on the flood coverage for the 02/03/2019–07/04/2019 observation period. The histogram is calculated based on all available Synthetic Aperture Radar (SAR) and optical data (black), as well only with SAR data (red).

Figure 14 shows the Backward Flood Duration at the flood peak on 19/03/2019, computed with a pixel spacing of 10 m. At this stage, the central and southern parts of the study area, in particular, had already been flooded for 7 days prior to the landfall of Idai on the night between the 14th and the 15th of March in 2019.

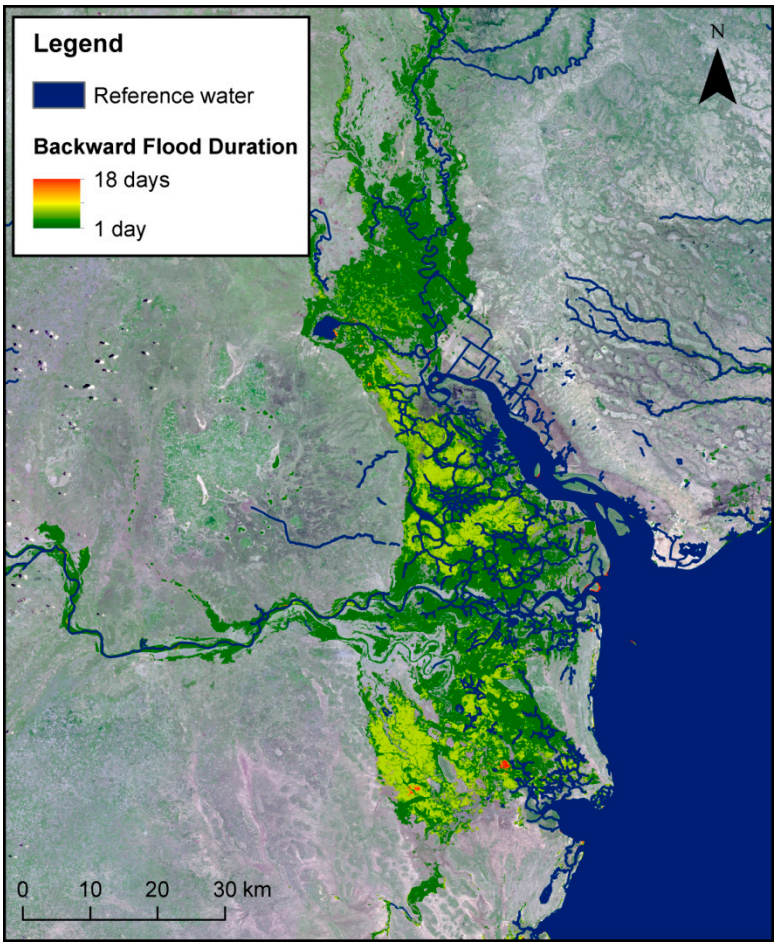

Figure 14. Backward Flood Duration calculated over the study area in Mozambique for the 02/03/2019–19/03/2019 observation period. The reference water extent is based on SWBD and data from HOT. A mosaic of four Sentinel-2 tiles (RGB) acquired on 02/12/2018 and 02/12/2018 is used as a background.

The histogram of the Total Flood Duration (Figure 15) shows a flooded area of more than 2500 km² during the observation period. More than 1000 km² was flooded for a short period of time (1–2 days). Overall, an area of more than 1700 km² was flooded for less than one week (1–7 days), whereas other areas were flooded for longer periods of time. In total, more than 600 km² were flooded over 1–2 weeks and ~130 km² over 2–3 weeks.

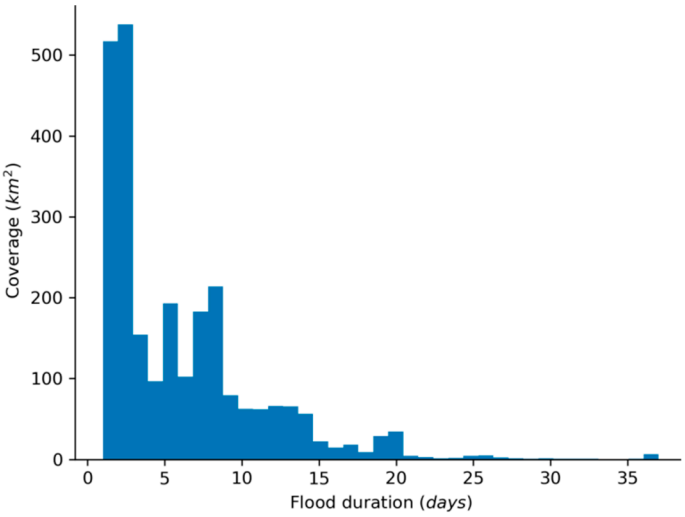

Figure 15. Histogram of Total Flood Duration calculated over the study area in Mozambique for the 02/03/2019–07/04/2019 observation period.

The dynamic nature of the inundated area during this flood event is visualized in Figure 16, which depicts the evolution of the total flooded area over time. For this purpose, 10 radar satellite images (9 Sentinel-1 and 1 TerraSAR-X) were used, which completely covered the area of interest (AOI). Since no completely cloud-free optical data set covering the whole AOI was available, no optical data was used in this particular example to compute the evolution of the flood extent.

The classification result of data from 14/03/2019 03:00 UTC shows that ~680 km² were already flooded before the landfall of the cyclone on 15/03/2019. The maximum flood extent of more than 1800 km² was detected on 19/03/2019. Between 20/03/2019 and 25/03/2019, the flooded area decreased drastically by more than 1400 km² within five days. Until the end of the observation period, the flood slowly decreased to ~100 km².

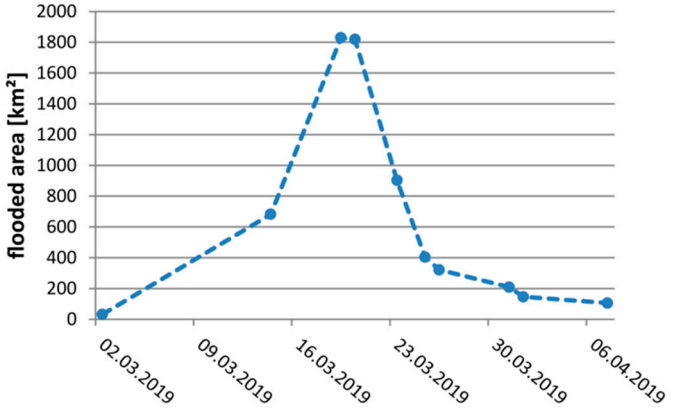

Figure 16. Evolution of the flooded area in the Mozambique study site derived from Sentinel-1 and TerraSAR-X data between 02/03/2019–07/04/2019.

4.2. India

The Total Flood Duration observed in Bihar (India) within the 03/07/2017–28/09/2017 observation period is visualized in Figure 17. The product was computed with a pixel spacing of 10 m. It can be seen that large areas were flooded for approximately 30–40 days, especially along and northwest of the Kosi River. Areas along the river courses were flooded for the whole observation period for up to 88 days. This was related to the fact that during the observation period, rivers carried more water than the time period upon which the seasonal reference water mask was based. This reference mask was derived from Sentinel-2 data during the dry period, which usually occurs

from November to April in this study area. Further details on generating the seasonal reference water mask from Sentinel-2 can be found in [16].

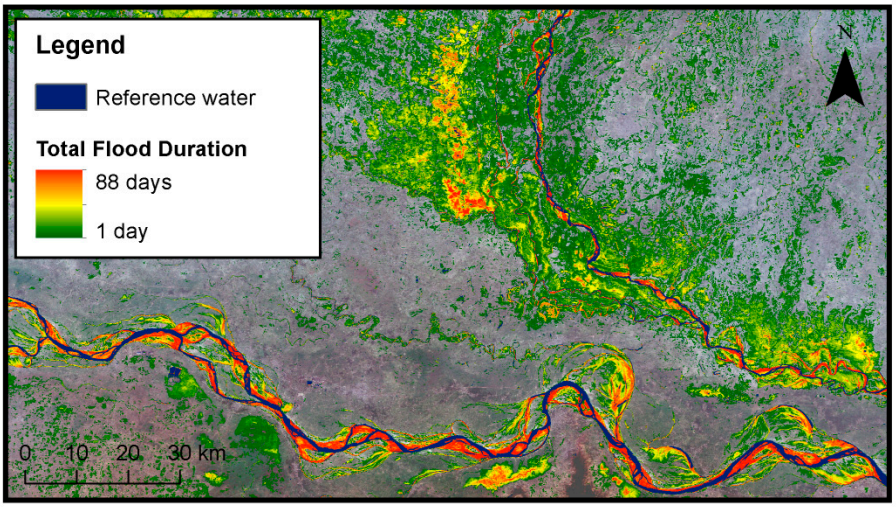

Figure 17. Total Flood Duration computed over the study area in Bihar for the 03/07/2017–28/09/2017 observation period. The reference water extent is generated from six Sentinel-2 observations acquired during the dry period over the same study area. A mosaic of two Sentinel-2 tiles (RGB) acquired on 29/12/2018 is used as a background.

Figure 18 depicts the corresponding quality layer. The median value of the quality layer of the Total Flood Duration was 26. This was significantly higher than the median value of 6 of the quality layer associated with the Total Flood Duration estimation in the study area located in Mozambique (Figure 12). Individual pixels had uncertainty values >80. The reason for this was related to the difference in observation frequencies over the two study areas. On average, acquisitions from at least one satellite every 1.5 days were available in the Mozambique study area, whereas acquisitions were only available every 3.5 days in the Bihar study area (Figure 2 and Figure 4).

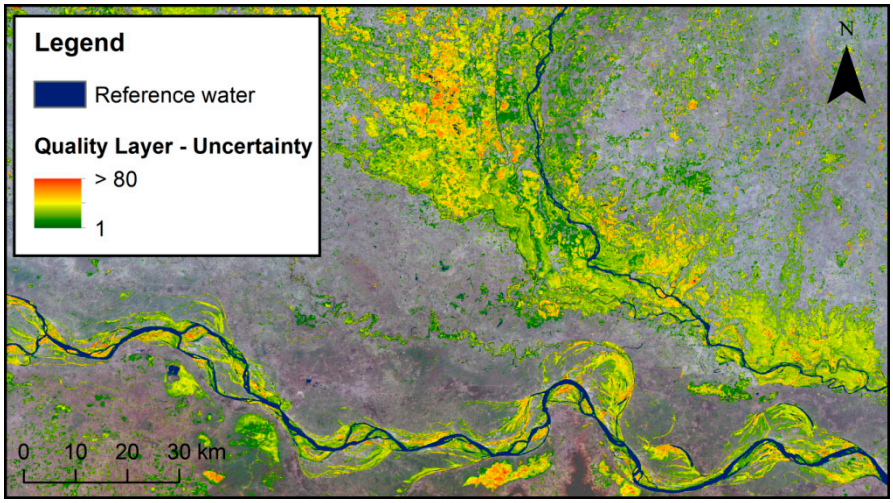

Figure 18. The associated quality layer derived over the study area in Bihar for the 03/07/2017–28/09/2017 observation period. The reference water extent is generated from six Sentinel-2 observations acquired during the dry period over the same study area. A mosaic of two Sentinel-2 tiles (RGB) acquired on 29/12/2018 is used as a background.

The Backward Flood Duration was computed for the peak of the flood event on 20/08/2017 with a pixel spacing of 10 m (Figure 19).

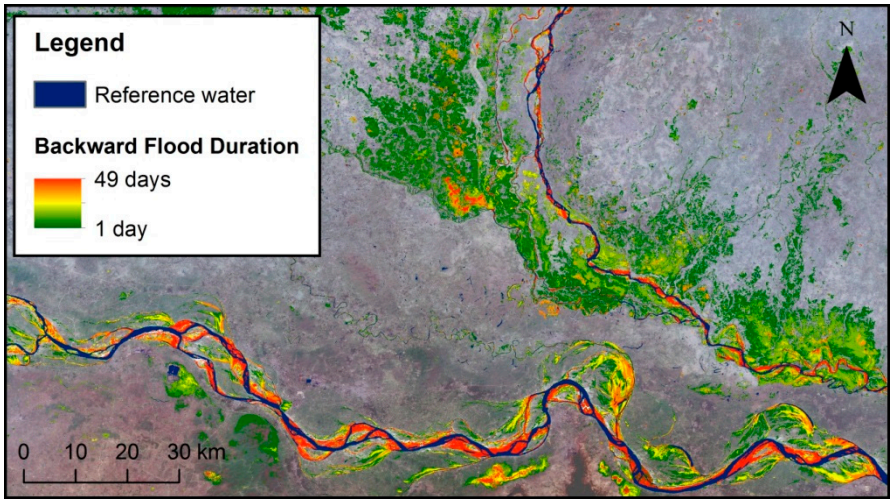

Figure 19. Backward Flood Duration computed over the study area in Bihar for the 03/07/2017–20/08/2017 observation period. The reference water extent is generated from six Sentinel-2 observations during the dry period. A mosaic of two Sentinel-2 tiles (RGB) acquired on 29/12/2018 is used as a background.

The histogram of the Total Flood Duration (Figure 20) provides more insights into the behavior of the flood event. In total, an area of more than 4600 km² was flooded during the observed time period. A large area of more than 1200 km² was flooded for just one day. More than half of the total area was flooded for less than one week (~2600 km²), whereas other areas were flooded for much longer periods, in particular, ~350 km² (2–3 weeks), ~420 km² (3–4 weeks), ~230 km² (4–5 weeks), ~240 km² (5–6 weeks), ~200 km² (6–7 weeks), ~80 km² (7–8 weeks), ~90 km² (8–9 weeks), ~50 km² (9–10 weeks), ~80 km² (10–11 weeks), ~130 km² (11–12 weeks) and ~30 km² (12–13 weeks). This highlights the large extent of the 2017 flood in Bihar. The results, moreover, indicate that some areas seemed to be flooded during the whole observation period. This is likely to be related to inconsistencies with the reference water mask, which did not cover areas permanently covered by water during the monsoon season.

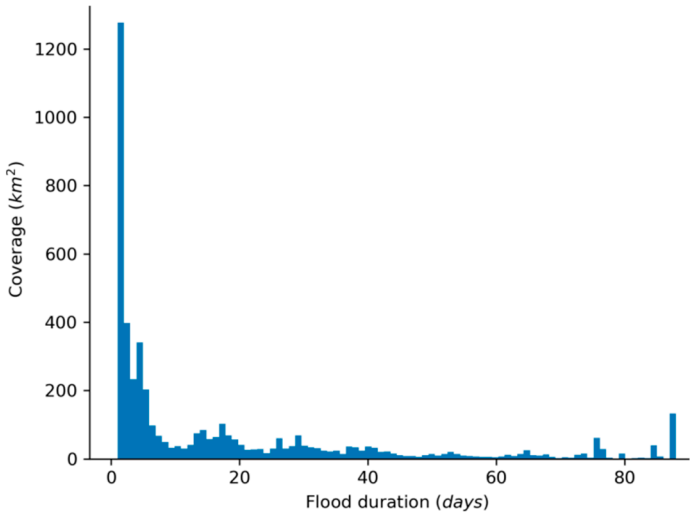

Figure 20. Histogram of Total Flood Duration computed for the study area in Bihar for the 03/07/2017–28/09/2017 observation period.

The dynamic nature of the flood event over time is illustrated in Figure 21. Fifteen Sentinel-1 satellite images were used and covered the whole study area. This prevented the introduction of biased information about the flood dynamic by using data that only partially covered the flooded area within the study area. The time-series of the flooded area shows that ~400 km² was inundated at

the beginning of the observation period. This highlights the fact that the seasonal reference water mask, which was derived with data from the dry period, was not covering the river courses that carried a larger quantity of water during the observation period. A small peak was detected at the beginning of the flood event on 15/07/2017, which corresponded with a flooded area of ~1120 km². The slight decrease in the next 12 days was followed by a rise to the maximum peak at ~2600 km² within 24 days. In the following month, the flooded area decreased again to ~630 km².

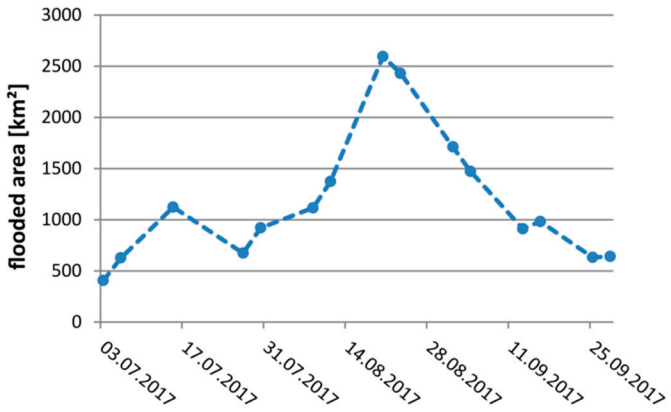

Figure 21. Evolution of the flooded area in Bihar derived from Sentinel-1 data acquired between 03/07/2017 and 28/09/2017.

5. Discussion

We presented an automated, end-to-end solution for flood duration estimation that is designed for operational use, from data ingestion to product delivery. Compared to other studies, the proposed method not only enables the timely analysis of long and dense time-series with a large number of scenes but also significantly contributes to satellite-based emergency mapping activities, where rapid analysis over synoptic areas and across diverse data sources is a crucial criterion. Flood duration products have not been considered in the context of emergency mapping to date, due to a lack of automation of existing methods [20–22] and often limited data availability from the onset of a disaster. Existing studies have not specifically considered this aspect and focused only on using data from single sensors [22–26,29,30] or sensors groups of optical [27] or SAR [20,21] missions.

In response, the proposed method focuses specifically on leveraging the use of data from multiple sensors (Sentinel-1, Sentinel-2, Landsat-8 and TerraSAR-X) and sensor groups (SAR and optical) simultaneously, to increase the temporal resolution of flood duration estimates and, hence, reduce associated uncertainties in the time-series analysis. For both study areas, we could show improvements in the quality metric when combining data from different sources; the results highlight the added value of the proposed multi-sensor approach. Since the flood duration method is highly independent on the source of the underlying flood extent masks, results from other satellite sensors and flood mapping methods can be used to further improve the temporal resolution as needed.

Furthermore, we considered the effect of invalid observations due to partial cloud or cloud shadow coverage at the pixel level rather than at the dataset level to limit their influence on temporal uncertainty. Consequently, the study takes a first step towards understanding and quantifying aggregated uncertainties associated with the temporal revisit period of the satellites and the impact of partial visibility in optical data due to atmospheric effects on the final product. The proposed quality layer shows relative uncertainties that reflect the dual contribution of observation frequency and the distribution of available acquisitions. The quality layer supports the comparability of different flood events with variable durations by averaging the co-period uncertainty by the number of observation gaps. However, further research is needed to also consider the classification accuracy of the input flood extent masks in the quality layer. These first results already show that the quality of the reference water mask clearly influences the flood duration estimation. An appropriate definition

and generation of a suitable reference water mask is, therefore, an important line of investigation for future research. This is of particular importance in highly dynamic environments, especially where surface waters are seasonally-affected.

The results illustrate the utility of two flood duration products towards more comprehensive flood monitoring at specific locations over time. In particular, the Backward Flood Duration can be used as an indicator of the duration of an ongoing flood event in days and, thus, provides information about flood persistence. This information is especially useful to consider, for example, to improve the coordination of relief supply activities undertaken by humanitarian aid organizations. The Total Flood Duration, on the other hand, is particularly useful for addressing scientific questions of the long-term comparison of annually recurring hydrological phenomena. Moreover, despite the focus of the presented work on temporary flooded areas and their dynamics, the method is generic enough to be adapted and applied to other similar phenomena. Further applications can include, but are not limited to, more generalized analysis of surface water body dynamics, temporal analysis of agricultural cycles or the evolution of burnt areas as a part of a fire monitoring system.

6. Conclusion

In this study, a fully automated method to estimate flood duration in near real-time is introduced based on the use of multi-sensor satellite data. The flood duration estimation builds on existing processing chains for the near real-time extraction of flood masks from Sentinel-1, Sentinel-2, Landsat-8 and TerraSAR-X. The combined use of data from different sensors enables higher observation frequency, which is instrumental in operational contexts and increases the reliability of flood duration estimates.

Two different kinds of flood duration products are developed to provide near real-time information about the duration of an ongoing flood event within a Backward Flood Duration layer and the total duration of flood coverage for a pre-defined time period, which could potentially cover several flood events. To quantify the uncertainty related to these products, quality layers are produced that account for the temporal revisit period of the virtual satellite constellation used, the distribution of observations and the presence of invalid pixels.

The proposed method is demonstrated on two flood events that occurred in 2019 in Sofala, Mozambique and in 2017 in Bihar, India, respectively. The derived products demonstrate skill in performing long-term investigations to monitor surface water dynamics and annually recurring hydrological extreme events. The results of the study highlight the utility of the products to further support satellite-based emergency mapping activities.

Author Contributions: Conceptualization, M.R. and S.M.; methodology, M.R. and S.M.; software, M.R.; formal analysis, M.R.; investigation, M.R, S.M. and M.W..; data curation, M.R., S.M. and M.W.; writing—original draft preparation, M.R., S.M. and M.W.; writing—review and editing, S.M. and M.W.; visualization, M.R., S.M. and M.W.; supervision, S.M. All authors have read and agreed to the published version of the manuscript.

Funding: This work was financed by DLR-internal funding and supported by the German Society for International Cooperation (GIZ) GmbH as part of the InsuResilience project (Grant No. 81220843).

Acknowledgments: The authors would like to thank the "Information Systems and Geomatics" team of the "Geo-Risks and Civil Security" department of the German Remote Sensing Data Center (DFD) for their technical support and two anonymous reviewers for their helpful comments and constructive suggestions.

Conflicts of Interest: The authors declare no conflict of interest.

References

1. Pulvirenti, L.; Pierdicca, N.; Chini, M.; Guerriero, L. An algorithm for operational flood mapping from synthetic aperture radar (SAR) data based on the fuzzy logic. *Nat. Hazards Earth Syst. Sci.* **2011,** *11*, 529-540.
2. Pulvirenti, L.; Chini, M.; Pierdicca, N.; Boni, G. Use of SAR data for detecting floodwater in urban and agricultural areas: The role of the interferometric coherence. *IEEE Trans. Geosci. Remote Sens*. **2015**, *54*, 1532-1544.

3. Huang, X.; Tan, H.; Zhou, J.; Yang, T.; Benjamin, A.; Wen, S.W.; Li, S.; Liu, A.; Li, X.; Fen, S. and et al. Flood hazard in Hunan province of China: An economic loss analysis. *Nat. Hazards* **2008**, *47*, 65-73.
4. Sanyal, J.; Lu, X.X. Application of remote sensing in flood management with special reference to monsoon Asia: A review. *Nat. Hazards* **2004**, *33*, 283-301.
5. Martinis, S.; Künzer, C.; Twele, A. *Flood studies using Synthetic Aperture Radar data*. In Thenkabail, P.: Remote Sensing Handbook Volume III - Remote Sensing of Water Resources, Disasters, and Urban Studies, Taylor and Francis, Milton Park, Oxfordshire UK, 2015; pp. 145-173.
6. Wallemarq, P.; Below, R.; McLean, D. *UNISDR and CRED report: Economic losses, poverty & disasters (1998–2017)*; Centre for Research on the Epidemiology of Disasters (CRED), Brussels, Belgium, 2018; pp. 1-33.
7. Hellmuth, M.E.; Osgood, D.E.; Hess, U.; Moorhead, A.; Bhojwani, H. *Index insurance and climate risk: Prospects for development and disaster management*. International Research Institute for Climate and Society (IRI), Columbia University, New York, USA, 2009.
8. Chuvieco, E. *A review of remote sensing methods for the study of large wildland fires*. Megafires project ENV-CT96-0256. Universidad de Alcalá, Alcalá de Henares, Spain, 1997.
9. Feng, M.; Sexton, J.O.; Channan, S.; Townshend, J.R. A global, high-resolution (30-m) inland water body dataset for 2000: First results of a topographic–spectral classification algorithm. *Int. J. Digit. Earth* **2016**, *9*, 113–133.
10. Zhou, Y.; Dong, J.; Xiao, X.; Xiao, T.; Yang, Z.; Zhao, G.; Zou, Z.; Qin, Y. Open Surface Water Mapping Algorithms: A Comparison of Water-Related Spectral Indices and Sensors. *Water* **2017**, *9*, 256.
11. Twele, A.; Cao, W.; Plank, S.; Martinis, S. Sentinel-1 based flood mapping: A fully automated processing chain. *Int. J. Remote Sens.* **2016**, *37*, 2990-3004.
12. Martinis, S.; Twele, A.; Kersten, J. A fully automated TerraSAR-X based flood service. *Isprs J. Photogramm. Remote Sens.* **2015**, *104*, 203-212.
13. Pekel, J.F.; Cottam, A.; Gorelick, N.; Belward, A.S. High-resolution mapping of global surface water and its long-term changes. *Nature* **2016**, *540*, 418-422, doi:10.1038/nature20584.
14. Isikdogan, F.; Bovik, A.C.; Passalacqua, P. Surface Water Mapping by Deep Learning. *IEEE J. Sel. Top. Appl. Earth Obs. Remote Sens.* **2017**, *10*, 4909–4918.
15. Chen, Y.; Fan, R.; Yang, X.; Wang, J.; Latif, A. Extraction of Urban Water Bodies from High-Resolution Remote-Sensing Imagery Using Deep Learning. *Water* **2018**, *10*, 585.
16. Wieland, M.; Martinis, S. A modular processing chain for automated flood monitoring from multi-spectral satellite data. *Remote Sens.* **2019**, *11*, 2330.
17. Klemas, V. Remote sensing of floods and flood-prone areas: An overview. *J. Coast. Res.* **2015**, *314*, 1005–1013.
18. Lin, L.; Di, L.; Yu, E.G.; Kang, L.; Shrestha, R.; Rahman, M.S.; Tang, J.; Deng, M.; Sun, Z.; Zhang, C. and et al. A review of remote sensing in flood assessment. Proceedings of the Fifth International Conference on Agro-Geoinformatics, Tianjin, China, 18-20 July 2016; 1-4.
19. Matgen, P.; Hostache, R.; Schumann, G.; Pfister, L.; Hoffmann, L.; Savenije, H.H.G. Towards an automated SAR-based flood monitoring system: Lessons learned from two case studies. *Phys. Chem. EarthParts A/B/C* **2011**, *36*, 241-252.
20. Bhatt, C.M.; Rao, G.S.; Farooq, M.; Manjusree, P.; Shukla, A.; Sharma, S.V.S.P.; Kulkarni, S.S.; Begum, A.; Bhanumurthy, V.; Diwakar, P.G. and et al. Satellite-based assessment of the catastrophic Jhelum floods of September 2014, Jammu & Kashmir, India. *Geomat. Nat. Hazards Risk* **2017**, *8*, 309-327.
21. Rahman, M.; Ningsheng, C.; Islam, M.M.; Dewan, A.; Iqbal, J.; Washakh, R.M.A.; Shufeng, T. Flood Susceptibility Assessment in Bangladesh Using Machine Learning and Multi-criteria Decision Analysis. *Earth Syst. Environ.* **2019**, *3*, 585-601.
22. Ramsey, E.; Lu, Z.; Suzuoki, Y.; Rangoonwala, A.; Werle, D. Monitoring duration and extent of storm-surge and flooding in western coastal Louisiana marshes with Envisat ASAR data. *IEEE J. Sel. Top. Appl. Earth Obs. Remote Sens.* **2011**, *4*, 387-399.
23. O'Hara, R.; Green, S.; McCarthy, T. The agricultural impact of the 2015–2016 floods in Ireland as mapped through Sentinel 1 satellite imagery. *Ir. J. Agric. Food Res.* **2019**, *58*, 44-65.
24. Kundu, S.; Aggarwal, S.P.; Kingma, N.; Mondal, A.; Khare, D. Flood monitoring using microwave remote sensing in a part of Nuna river basin, Odisha, India. *Nat. Hazards* **2015**, *76*, 123-138.

25. Rahman, M.R.; Thakur, P.K. Detecting, mapping and analysing of flood water propagation using synthetic aperture radar (SAR) satellite data and GIS: A case study from the Kendrapara District of Orissa State of India. *Egypt. J. Remote Sens. Space Sci.* **2018**, *21*, 37-41.
26. Zhang, L.; Yu, W.; Li, G.; Zhang, H. An approach for flood inundated duration extraction based on Level Set Method using remote sensing data. Proceedings of the International Geoscience and Remote Sensing Symposium, Beijing, China, 10-15 July 2016; 1820-1822.
27. Kumar, R. Flood hazard assessment of 2014 floods in Sonawari sub-district of Bandipore district (Jammu & Kashmir): An application of geoinformatics. *Remote. Sen. Appl. Soc. Environ.* **2016**, *4*, 188-203.
28. Graf, W.L. Locational probability for a dammed, urbanizing stream: Salt River, Arizona, USA. *Environ. Manage.* **2000**, *25*,321-335.
29. Kurte, K.; Potnis, A.; Durbha, S. Semantics-enabled Spatio-Temporal Modeling of Earth Observation Data: An application to Flood Monitoring. Proceedings of the 2nd ACM SIGSPATIAL International Workshop on Advances on Resilient and Intelligent Cities, Chicago, USA, 5 November 2019; 41-50.
30. Islam, A.S.; Bala, S.K.; Haque, M.A. Flood inundation map of Bangladesh using MODIS time-series images. *J. Flood Risk Manage.* **2010**, *3*, 210-222.
31. United Nations Office for the Coordination of Humanitarian Affairs. Available online: https://www.unocha.org/southern-and-eastern-africa-rosea/cyclones-idai-and-kenneth (accessed on 16 December 2019).
32. NASA JPL. NASA Shuttle Radar Topography Mission Global 1 arc second [Data set]. NASA EOSDIS Land Processes DAAC, 2013. https://doi.org/10.5067/MEaSUREs/SRTM/SRTMGL1.003 (accessed on 19 December 2019).
33. Martinis, S.; Twele, A.; Voigt, S. Towards operational near real-time flood detection using a split-based automatic thresholding procedure on high resolution TerraSAR-X data. *Nat. Hazards Earth Syst. Sciences.* **2019**, *9*, 303-314.
34. Martinis, S.; Plank, S.; Cwik, K. The use of Sentinel-1 time-series data to improve flood monitoring in arid areas. *Remote Sens.* **2018**, *10*, 583.
35. Carroll, M.; Townshend, J.; DiMiceli, C.; Noojipady, P.; Sohlberg, R. A new global raster water mask at 250 meter resolution. *Int. J. Digital Earth*, **2009**, *2*, 291–308.
36. Martinis, S.; Twele, A.; Strobl, C.; Kersten, J.; Stein, E. A multi-scale flood monitoring system based on fully automatic MODIS and TerraSAR-X processing chains. *Remote Sens.* **2013**, *5*, 5598-5619.
37. Wieland, M.; Martinis, S.; Li, Y. Multi-sensor cloud and cloud shadow segmentation with a convolutional neural network. *Remote Sens. Environ.* **2019**, *230*, 1–12.